Showcasing research from the group of Priv.-Doz. Dr Goran Angelovski, MR Neuroimaging Contrast Agents, Max Planck Institute for Biological Cybernetics, Tübingen, Germany. This illustration is designed by Dr Giuseppe Gambino.

A ratiometric ^{19}F MR-based method for the quantification of Ca^{2+} using responsive paramagnetic probes

A combination of para- and diamagnetic lanthanide complexes enables the absolute quantification of Ca^{2+} concentration *via* a ratiometric ^{19}F MRI methodology.

As featured in:
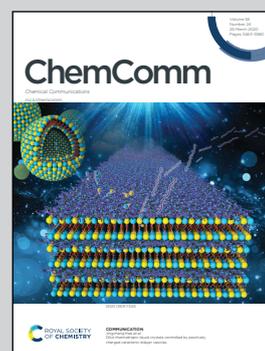
ChemComm
Chemical Communications

ROYAL SOCIETY OF CHEMISTRY

rsc.li/chemcomm

Check for updates

A ratiometric ^{19}F MR-based method for the quantification of Ca^{2+} using responsive paramagnetic probes†

Giuseppe Gambino, [iD] [a] Tanja Gambino, [iD] [a] Rolf Pohmann[b] and
Goran Angelovski [iD] *[a]

We present a method for assessing the extracellular calcium concentration using ^{19}F chemical shift imaging. Specifically, a custom made calcium-responsive and lanthanide-based ^{19}F MRI probe that undergoes a strong and highly specific modulation of its signal upon coordination with calcium ions was developed and its performance is presented.

Magnetic resonance imaging (MRI) is a powerful and widely used technique, able to provide three-dimensional anatomical images with excellent spatial resolution. However, it proves challenging to extrapolate further information about the voxel-wise composition of the signal and the specific nuclei from which it originates. On the other hand, magnetic resonance spectroscopy (MRS) allows acquisition of localized mono-dimensional (1D) MR spectra, while with chemical shift imaging (CSI) it is possible to obtain a spatial distribution of chemical shifts in a three-dimensional sample.[1–3] Using these techniques, a very detailed image of the investigated tissue can be obtained, without losing any spatial information. To this end, ^{1}H MRS has significantly contributed in providing meaningful insights into metabolic activity, particularly in the brain.[4]

By providing the localized 1D proton spectra of different metabolites with their specific chemical shifts,[5] this technique enables the following of biological processes by monitoring the distribution and concentration of such metabolites in the tissue. However, because of the narrow spectral width of the proton frequencies, signals of metabolites usually result in complex spectra that are difficult to resolve, in particular in the region between 2 and 3 ppm. Other nuclei, such as ^{31}P and ^{13}C, are also exploited in MRS.[6] Yet, both present major drawbacks, such as lower sensitivity compared to proton nuclei (both ^{31}P and ^{13}C),

low isotopic abundance (^{13}C), or absence in many biomolecules (^{31}P). Moreover, the MRS methods mentioned above are suitable only for organic biomolecules and metabolites that contain ^{1}H, ^{13}C or ^{31}P nuclei, while they are unsuitable for endogenous metal ion targets.

Exploiting ^{19}F represents an excellent alternative with high potential for *in vivo* MRI, MRS and CSI.[7] Primarily, its high natural isotopic abundance and relative sensitivity are comparable to those of protons. Although the negligible endogenous concentration of ^{19}F prevents its use in the direct investigation of biological processes, the lack of background signal is advantageous and can be exploited to develop tracers that yield high signal-to-noise ratios (SNR). Following this idea, emulsions of highly fluorinated molecules have been successfully used for labelling and subsequently tracking cells *in vivo* using MRI.[8–10] Furthermore, ^{19}F is extremely sensitive to changes in its microenvironment on a chemical and electronic level, with an NMR resonance frequency range that is quite wide. Thus exploiting the relaxation properties, chemical shift and chemical exchange variations led to the development of responsive systems to measure tissue pO_2, and detect ions, pH and enzymatic activity *via* various triggering mechanisms.[7,11,12]

Monitoring of fluctuations in the concentration of endogenous metal ions is a particularly interesting application because of their role and relevance in the signalling and regulation of numerous biological processes. By using responsive,[13] or so-called smart contrast agents (SCAs), a functional MRI (fMRI) method that operates at the ^{1}H frequency demonstrated considerable potential for the assessment of neuronal activity by detecting the intracellular and extracellular calcium concentrations.[14,15] Importantly, the capability of Ca-sensitive SCAs to monitor cerebral ischemia has also been presented, thus showing significant recent advancements in this field and great prospects of molecular fMRI for contemporary biomedical research and applications.[16]

In parallel, the susceptibility of ^{19}F nuclei has promoted the development of probes that can detect metal ions through changes in their chemical shift.[17,18] The ^{19}F chemical exchange saturation transfer (CEST) investigations built upon this early

[a] *MR Neuroimaging Agents, MPI for Biological Cybernetics, Tuebingen, Germany.*
  E-mail: goran.angelovski@tuebingen.mpg.de
[b] *High-Field Magnetic Resonance, MPI for Biological Cybernetics, Tuebingen,*
  Germany

† Electronic supplementary information (ESI) available: Synthetic procedures and additional ^{19}F NMR and CSI experimental data. See DOI: 10.1039/c9cc09977h

work to result in an attractive methodology that allows multi-ion detection,[19,20] while self-assembled, ^{19}F-containing peptide amphiphiles were also used to quantify Ca^{2+} concentrations that are biologically relevant.[21] For ^{19}F MRI applications, however, high concentrations and shorter relaxation times of a fluorinated probe would be required to obtain sufficient signals within reasonable acquisition times.[7] One strategy to overcome this has been provided by combining fluorinated probes and paramagnetic ions at a short distance, usually within the same molecule.[22] The ability of paramagnetic ions to affect the relaxation properties and chemical shifts of the ^{19}F nuclei *via* paramagnetic relaxation enhancement (PRE) and pseudocontact shifts (PCS), respectively, has granted the possibility to exploit such phenomenon in the design of responsive systems for ^{19}F MRI and MRS.[11,23,24] Benefiting from these effects, a few SCAs have been designed and assessed. For instance, SCAs for the detection of enzymatic activity showed their great potential;[25–27] however, the response of these probes is irreversible due to the cleavage of the enzyme-specific linker. On the other hand, SCAs that are able to reversibly detect pH, Ca^{2+} or citrate anions have also been reported.[28–30] However, their sensitivity was partially compromised by the presence of multiple signals at different frequencies due to the presence of molecular isomers, in the case of cyclen-based complexes,[31] or a lower number of ^{19}F spins in the responsive molecule.

With the intention to take advantage of the current knowledge in probe design and to capitalize on the favourable features of ^{19}F MRI and MRS, we designed the ligand **L** that, when chelating paramagnetic lanthanide ions, can act as a calcium-responsive SCA (Fig. 1). To establish it as a probe suitable for future applications, we implemented a few significant improvements in the design of the sensor molecule. First, we used a lanthanide-cage based on the macrocyclic ligand 1,4-bis(carboxymethyl)-6-[bis(carboxymethyl)]-amino-6-methylperhydro-1,4-diazepine (AAZTA).[32] By selecting this chelator in the design of the SCA, we attempted to avoid additional ^{19}F NMR resonances; to date no isomeric distribution in the NMR-timescale has been reported for such compounds. To improve the sensitivity of the probe, we used perfluorinated *tert*-butylether as the fluorine-bearing group, attached by a flexible propyl chain to the calcium-chelating moiety (Fig. 1). By doing so, we functionalized our molecule with a remarkably high number

of spectroscopically equivalent ^{19}F nuclei per paramagnetic ion (nine), while maintaining the excellent water solubility of the complex. Finally, we selected the calcium chelator based on ethylene glycol-bis(β-aminoethyl ether)-*N,N,N′,N′*-tetraacetic acid (EGTA) as the part of the molecule responsible for the coordination of Ca^{2+}, due to its well investigated high specificity and affinity towards these ions when incorporated within the SCA.[30,33] The fluorinated ligand was obtained starting with the amide coupling of the amine **1** with bromoacetic acid (Scheme S1 in ESI†). The obtained bromide **2** was used to alkylate the secondary amine of **3**. Meanwhile, fluorinated amine **6** was coupled with bromoacetyl bromide to obtain fluorinated bromide **7**. Following hydrogenation of **4**, **7** was used to alkylate the newly obtained secondary amine of **5**, yielding a protected ligand **8**. Once the chelating molecule **L** was prepared by hydrolyzing *tert*-butyl esters with formic acid, we selected dysprosium as the paramagnetic ion for incorporation in the SCA, due to the high PCS effect and the optimal PRE properties of the ions.

Advantageously, the ^{19}F NMR spectra of **DyL** showed a single resonance at −72.7 ppm (Fig. 2b). Moreover, the obtained SNR value was as much as 5 times higher in comparison to those of compounds reported in the literature for the same concentration of metal ([Dy^{3+}] = 3.0 mM), due to the larger amount of fluorine atoms per lanthanide ion.[30] Subsequently, we assessed the response of the system to Ca^{2+} by titrating **DyL** with a solution of $CaCl_2$ and recording the ^{19}F NMR spectra (Fig. 2b and c). The obtained SNR of the ^{19}F NMR signal undergoes a massive 10-fold decrease under these conditions. Such a powerful response is due to the PRE effect, resulting in the significant shortening of the longitudinal and transverse ^{19}F relaxation times; the analogous changes in the ^{19}F relaxation times for **YL** were not pronounced (Table 1).

Concurrently, this effect is accompanied by the PCS and further shifting of the resonance frequency of the Ca^{2+}-bound complex (*ca.* −1 ppm). We hypothesize that both these effects
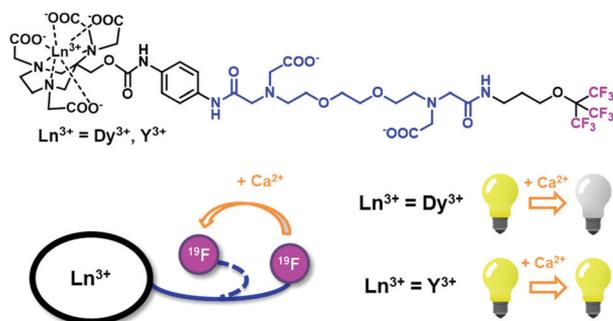

Fig. 1 Chemical structure of the reported complexes **DyL** and **YL** (top) and graphical illustration of the working principle of the responsive agent (bottom).
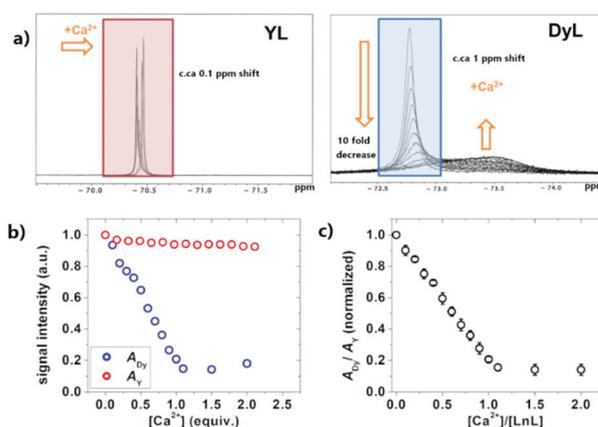

Fig. 2 ^{19}F NMR titration experiments with **DyL** and **YL**. (a) ^{19}F NMR spectra of **YL** (left) and **DyL** (right) in the presence of increasing [Ca^{2+}] (from 0 to 2.0 equiv.) measured at 7 T and 25 °C. (b) Signal intensity values for **YL** (A_Y, red area in the left panel) and **DyL** (A_{Dy}, blue area in the right panel) plotted as a function of increasing [Ca^{2+}]. (c) Average values for A_{Dy}/A_Y plotted against the normalized [Ca^{2+}] for a set of three samples containing **DyL** and **YL** in ratios of 50:50, 75:25 and 90:10 ([Dy] = 2.0 mM), measured at 7 T and 25 °C.

Table 1 ^{19}F T_1 and T_2 relaxation times for **DyL** and **YL** in the absence and presence of Ca^{2+} (1 equiv.) at 7 T, 25 °C and pH 7.4 (50 mM HEPES)

Complex	T_1 (ms)	T_2 (ms)
DyL only/+ Ca^{2+}	157/127	17/6
YL only/+ Ca^{2+}	1320/1190	543/454

Fig. 3 Averaged ^{19}F MRS spectra of phantom tubes **1–6** [**DyL**] = 5.0 mM/ [**YL**] = 0.5 mM in 50 mM HEPES pH 7.4, [Ca^{2+}]$_{eq}$ = 0.0 (**1**), 0.2 (**2**), 0.4 (**3**), 0.6 (**4**), 0.8 (**5**), and 1.0 (**6**); obtained by recording a three-dimensional CSI dataset at 7 T.

Fig. 4 CSI on the phantom tubes containing a mixture of **DyL** and **YL** in 10 : 1 ratio (5.5 mM total [**DyL** + **YL**]) in the presence of 0.0, 0.2, 0.4, 0.6, 0.8 and 1.0 equivalents of Ca^{2+} in tubes 1–6, respectively. (a) Normalized CSI image of A_{Dy}/A_Y; the side bar shows the A_{Dy}/A_Y values. (b) Quantitative [Ca^{2+}] map obtained by fitting the ratiometric data; the side bar shows the obtained [Ca^{2+}] in mM.

are the result of a contraction of the distance between the perfluorinated group and the paramagnetic centre, as a consequence of the structural rearrangement that occurs upon coordination of the Ca^{2+} ion. This assumption is corroborated by characterizing the ^{19}F NMR signal behaviour of the diamagnetic Y^{3+} analogue **YL**. Indeed, by exchanging the paramagnetic ion for a diamagnetic one, we observed virtually no effect on the coordination of the Ca^{2+} ion on the chemical shift (<0.1 ppm) and signal intensity of the ^{19}F NMR signal (Fig. 2a). Also, **DyL** did not show any interaction with Mg^{2+}, while it proved able to coordinate Zn^{2+} (Fig. S2 in the ESI†). However, this phenomenon presents no problem for this methodology, because of the much lower concentration of Zn^{2+} in the brain extracellular space.[34]

By obtaining Ca^{2+}-independent or -dependent ^{19}F NMR signals for **YL** and **DyL**, respectively, we were able to quantify variations in [Ca^{2+}] by using the signal of the former as the internal reference for changes in the signal of the latter probe. To this end, we titrated a mixture of **DyL** and **YL** in three different ratios (50 : 50, 70 : 30 and 90 : 10, respectively) with CaCl$_2$, while maintaining the concentration of [**DyL**] (2.0 mM). We recorded the ^{19}F NMR spectra after every addition of Ca^{2+}, and integrated the regions between −70.0 and −70.5 ppm (A_Y) and between −72.5 and −73.0 ppm (A_{Dy}) to obtain the signal intensity of **YL** and **DyL**, respectively. Subsequently, we calculated the A_{Dy}/A_Y for every titration point, and plotted the normalized values of the three titrations against the [Ca^{2+}] (Fig. 2c and Fig. S3–S6 in ESI†). Importantly, the behaviour of the complexes is very consistent and independent of their ratio and their total concentration.

To further explore the potential of this method, we prepared a set of phantom tubes containing a mixture of **DyL** and **YL** in 10 : 1 ratio (5.5 mM total [**DyL** + **YL**]) in the presence of 0.0, 0.2, 0.4, 0.6, 0.8 and 1.0 equivalents of Ca^{2+}, and performed CSI measurements in a 7 T MRI scanner (Fig. S7 in the ESI†).

This allowed us to complete a voxel-wise analysis of the obtained ^{19}F MR spectra and images, thus revealing the potential application in functional molecular imaging studies (Fig. 3 and 4). We first averaged the ^{19}F spectra for each sample from the CSI image. In analogy to the ^{19}F NMR experiments, the signal intensity of the **DyL** resonance decreased with increasing [Ca^{2+}]; however, it remained constant under all conditions at the **YL** frequency (Fig. 3).

We then processed the acquired CSI dataset by computing the A_{Dy} and A_Y values to provide a voxel-wise map of their ratio for applying a linear fit to the data obtained from the ^{19}F NMR titration experiments (Fig. 2c and Fig. S6 in the ESI†), and we could correlate the concentration of Ca^{2+} according to eqn (1), where A_{Dy}/A_Y is the normalized ratio of **DyL** and **YL** signals, a and b are values obtained from the fit, and [Ca^{2+}]$_{eq}$ is the concentration of Ca^{2+} expressed in equivalents. Subsequently, we multiplied the calculated [Ca^{2+}]$_{eq}$ value with [**DyL** + **YL**] used

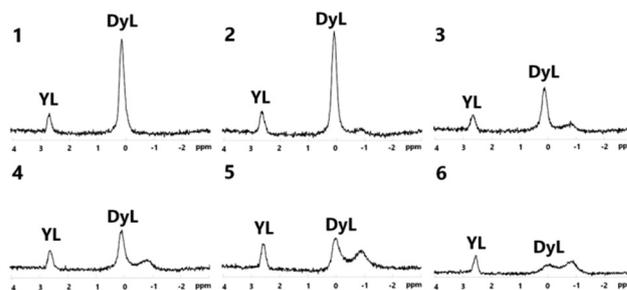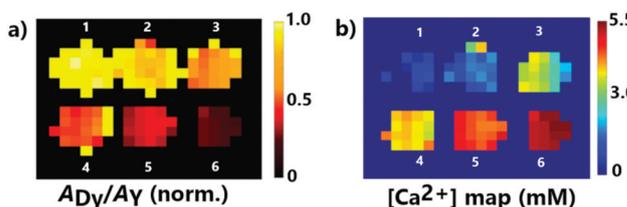in this measurement (5.5 mM) for each voxel. We obtained a voxel-wise concentration map of the absolute [Ca^{2+}] expressed in mM, which was in excellent agreement with the actual Ca^{2+} concentration used in each sample (Fig. 4b and Table S3 in the ESI†).

$$\frac{A_{Dy}}{A_Y} = b \cdot \left[Ca^{2+}\right]_{eq} + a \qquad (1)$$

In turn, this method proved to be fully quantitative under all conditions where [**DyL**] ≥ [Ca^{2+}] and [**YL**] is detectable. Specifically, due to the ability of ^{19}F MRI to quantify the amount of ^{19}F spins,[10] the method presented here can achieve the determination of overall probe concentration *via* the fluorine resonance in **YL**, while the resonance of **DyL** and its variable signal will aid the quantification of the Ca^{2+} concentration. This specific and very important feature of the methodology presented here could turn into an important tool for the absolute quantification of essential endogenous ions such Ca^{2+} or Zn^{2+} that exist in µM to mM concentrations,[34] since the abnormalities in their concentration may be indicative of various pathological conditions.[35,36] Also the majority of practical aspects for the implementation of this methodology should be fulfilled: despite the lower sensitivity of ^{19}F MRS/MRI, high amounts of ^{19}F nuclei in the reported SCA ensure common duration of the CSI recordings on the order of tens of minutes. Namely, the tests in the scanner were made with the acquisition time of 1 hour for a quite large field of view (80 × 80 mm) and a very good signal-to-noise ratio (SNR) of >60

was obtained for 10% of **YL** in each sample. Considering this high SNR, the CSI acquisition could be reduced a few times with still improved spatial resolution, while providing good quality data to support the necessary conclusions.

We report a methodology that is highly advantageous for potential *in vivo* utilization. Generally, variations in the concentration of the probe and the inability to quantify it in biological tissues currently represent a major hindrance for the application of responsive CAs *in vivo*. However, our method has the capacity to circumvent most of these obstacles: it deals with a pair of highly specific Ca-variable and -invariable signals, the latter allowing easy quantification of the SCA, while not requiring the exact binding affinity constants to successfully determine the $[Ca^{2+}]$. The two ^{19}F signals are generated by two chemically different probes, which should have virtually identical biocompatibility and behaviour *in vivo* (*i.e.* diffusion rate, stability, interaction with tissue and excretion). Moreover, the high number of fluorine atoms per SCA and the acquisition of a single resonance can ensure signal detection after acquisition times at the level of minutes. Additionally, the developed mechanism could be employed for the design of SCAs suitable for other metal ions and molecular targets, provided that the sensor or recognition moiety is appropriately adjusted. Overall, the approach shown here represents an incredibly attractive perspective to overcome some of the main obstacles to the use of SCAs *in vivo*. The possibility to obtain spatially resolved maps of $[Ca^{2+}]$ in a tissue would represent a great leap towards a better understanding of numerous pathological and biological processes such as ischemia and neural activity, defining a substantial step forward for contemporary molecular functional imaging studies.

Conflicts of interest

There are no conflicts to declare.

Notes and references

1 L. Brateman, *Am. J. Roentgenol.*, 1986, **146**, 971–980.
2 T. R. Brown, B. M. Kincaid and K. Ugurbil, *Proc. Natl. Acad. Sci. U. S. A.*, 1982, **79**, 3523–3526.
3 A. Haase, J. Frahm, W. Hanicke and D. Matthaei, *Phys. Med. Biol.*, 1985, **30**, 341–344.
4 J. Frahm and F. Hanefeld, *Neuropediatrics*, 1996, **27**, 64–69.
5 P. S. Allen, R. B. Thompson and A. H. Wilman, *NMR Biomed.*, 1997, **10**, 435–444.
6 P. C. M. Van Zijl and P. B. Barker, *Ann. N.Y. Acad. Sci.*, 1997, **820**, 75–96.
7 J.-X. Yu, R. R. Hallac, S. Chiguru and R. P. Mason, *Prog. Nucl. Magn. Reson. Spectrosc.*, 2013, **70**, 25–49.
8 J. M. Janjic and E. T. Ahrens, *WIREs Nanomed. Nanobiotechnol.*, 2009, **1**, 492–501.
9 M. Srinivas, A. Heerschap, E. T. Ahrens, C. G. Figdor and I. J. M. D. Vries, *Trends Biotechnol.*, 2010, **28**, 363–370.
10 M. Srinivas, P. Boehm-Sturm, C. G. Figdor, I. J. de Vries and M. Hoehn, *Biomaterials*, 2012, **33**, 8830–8840.
11 K. L. Peterson, K. Srivastava and V. C. Pierre, *Front. Chem.*, 2018, **6**, 160.
12 M. Yu, B. S. Bouley, D. Xie, J. S. Enriquez and E. L. Que, *J. Am. Chem. Soc.*, 2018, **140**, 10546–10552.
13 M. C. Heffern, L. M. Matosziuk and T. J. Meade, *Chem. Rev.*, 2014, **114**, 4496–4539.
14 S. Okada, B. B. Bartelle, N. Li, V. Breton-Provencher, J. J. Lee, E. Rodriguez, J. Melican, M. Sur and A. Jasanoff, *Nat. Nanotechnol.*, 2018, **13**, 473–477.
15 A. Barandov, B. B. Bartelle, C. G. Williamson, E. S. Loucks, S. J. Lippard and A. Jasanoff, *Nat. Commun.*, 2019, **10**, 897.
16 T. Savić, G. Gambino, V. S. Bokharaie, H. R. Noori, N. K. Logothetis and G. Angelovski, *Proc. Natl. Acad. Sci. U. S. A.*, 2019, **116**, 20666–20671.
17 G. A. Smith, R. T. Hesketh, J. C. Metcalfe, J. Feeney and P. G. Morris, *Proc. Natl. Acad. Sci. U. S. A.*, 1983, **80**, 7178–7182.
18 H. L. Kirschenlohr, J. C. Metcalfe, P. G. Morris, G. C. Rodrigo and G. A. Smith, *Proc. Natl. Acad. Sci. U. S. A.*, 1988, **85**, 9017–9021.
19 A. Bar-Shir, A. A. Gilad, K. W. Y. Chan, G. S. Liu, P. C. M. van Zijl, J. W. M. Bulte and M. T. McMahon, *J. Am. Chem. Soc.*, 2013, **135**, 12164–12167.
20 A. Bar-Shir, N. N. Yadav, A. A. Gilad, P. C. M. van Zijl, M. T. McMahon and J. W. M. Bulte, *J. Am. Chem. Soc.*, 2015, **137**, 78–81.
21 A. T. Preslar, L. M. Lilley, K. Sato, S. R. Zhang, Z. K. Chia, S. I. Stupp and T. J. Meade, *ACS Appl. Mater. Interfaces*, 2017, **9**, 39890–39894.
22 K. H. Chalmers, E. De Luca, N. H. M. Hogg, A. M. Kenwright, I. Kuprov, D. Parker, M. Botta, J. I. Wilson and A. M. Blamire, *Chem. – Eur. J.*, 2010, **16**, 134–148.
23 I. Bertini, C. Luchinat and G. Parigi, *Prog. Nucl. Magn. Reson. Spectrosc.*, 2002, **40**, 249–273.
24 P. Harvey, I. Kuprov and D. Parker, *Eur. J. Inorg. Chem.*, 2012, 2015–2022.
25 S. Mizukami, R. Takikawa, F. Sugihara, Y. Hori, H. Tochio, M. Walchli, M. Shirakawa and K. Kikuchi, *J. Am. Chem. Soc.*, 2008, **130**, 794–795.
26 S. Mizukami, H. Matsushita, R. Takikawa, F. Sugihara, M. Shirakawa and K. Kikuchi, *Chem. Sci.*, 2011, **2**, 1151–1155.
27 A. Keliris, I. Mamedov, G. E. Hagberg, N. K. Logothetis, K. Scheffler and J. Engelmann, *Contrast Media Mol. Imaging*, 2012, **7**, 478–483.
28 A. M. Kenwright, I. Kuprov, E. De Luca, D. Parker, S. U. Pandya, P. K. Senanayake and D. G. Smith, *Chem. Commun.*, 2008, 2514–2516.
29 P. Harvey, K. H. Chalmers, E. De Luca, A. Mishra and D. Parker, *Chem. – Eur. J.*, 2012, **18**, 8748–8757.
30 P. Kadjane, C. Platas-Iglesias, P. Boehm-Sturm, V. Truffault, G. E. Hagberg, M. Hoehn, N. K. Logothetis and G. Angelovski, *Chem. – Eur. J.*, 2014, **20**, 7351–7362.
31 K. J. Miller, A. A. Saherwala, B. C. Webber, Y. Wu, A. D. Sherry and M. Woods, *Inorg. Chem.*, 2010, **49**, 8662–8664.
32 S. Aime, L. Calabi, C. Cavallotti, E. Gianolio, G. B. Giovenzana, P. Losi, A. Maiocchi, G. Palmisano and M. Sisti, *Inorg. Chem.*, 2004, **43**, 7588–7590.
33 G. Angelovski, P. Fouskova, I. Mamedov, S. Canals, E. Toth and N. K. Logothetis, *ChemBioChem*, 2008, **9**, 1729–1734.
34 G. G. Somjen, *Ions in the brain: normal function, seizures, and strokes*, Oxford University Press, New York, Oxford, 2004.
35 P. Marambaud, U. Dreses-Werringloer and V. Vingtdeux, *Mol. Neurodegener.*, 2009, **4**, 20.
36 M. C. McCord and E. Aizenman, *Front. Aging Neurosci.*, 2014, **6**, 77.